ACS APPLIED MATERIALS & INTERFACES

Research Article

www.acsami.org

Plasmonic Nanobiosensor Based on Hairpin DNA for Detection of Trace Oligonucleotides Biomarker in Cancers

Yanling Hu,[†,§] Lei Zhang,*[,†,§] Ying Zhang,[†] Bin Wang,[†] Yawei Wang,[†] Quli Fan,[†] Wei Huang,*[,†,‡] and Lianhui Wang*[,†]

[†]Key Laboratory for Organic Electronics and Information Displays & Institute of Advanced Materials, National Jiangsu Synergistic Innovation Center for Advanced Materials (SICAM), Nanjing University of Posts & Telecommunications, 9 Wenyuan Road, Nanjing 210023, China

[‡]Key Laboratory of Flexible Electronics (KLOFE) & Institute of Advanced Materials (IAM), National Jiangsu Synergistic Innovation Center for Advanced Materials (SICAM), Nanjing Tech University (NanjingTech), 30 South Puzhu Road, Nanjing 211816, China

Supporting Information

ABSTRACT: MicroRNAs (miRNAs), a class of small, endogenous, noncoding RNA molecules, can serve as biomarkers for potential applications in cancer diagnosis, prognosis, and prediction due to its abnormal expression. As a result, a novel label-free biosensor with nanometer scale was prepared and employed in the detection of trace oligonucleotides based on the localized surface plasmon resonance (LSPR). The dielectric constant on the surface of DNA modified gold nanoparticle would change when probe single-strand DNA hybridized with target oligonucleotides, which resulted in the notable red shift of scattering peak position. The biosensor with excellent selectivity can be used in a real-time monitoring hybridization process. Notably, this method provided label-free detection of DNA and miRNA at single nanoparticle level with limit of detection up to 3 nM. Due to the advantages of LSPR scattering spectra, single nanoparticle biosensor can be designed for trace cancer-relevant miRNAs detection in the future.

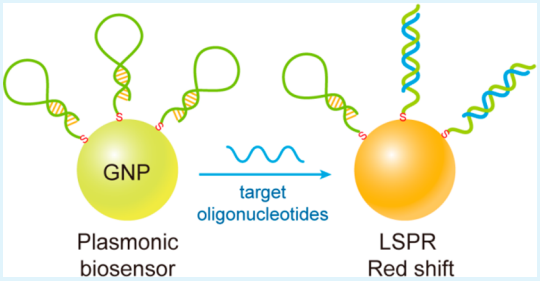

KEYWORDS: *surface plasmon resonance, biosensor, single gold nanoparticle, oligonucleotide detection*

INTRODUCTION

MicroRNAs (miRNAs) are small, endogenous, noncoding RNA molecules that are 20−24 nucleotides (nt) in length.[1] They play important roles in regulating gene expression by binding to the 3′ untranslated regions of target genes in various biological processes at the post-transcriptional level including early development, proliferation, cell apoptosis, and cell proliferation.[2,3] Abnormal expression of miRNAs has been demonstrated to be related to a range of cancers such as breast cancer,[4] lung cancer,[5] pancreatic cancer,[6] hepatocellular cancer,[7] colorectal cancer,[8] and glioblastoma,[9] which occurs in the precancerous stage as well as in malignant cells.[10] As an example, miRNA-21 was associated with all the cancers mentioned above and was observed to be upregulated more than 2-fold compared with normal tissues in the squamous cell lung carcinoma tissues.[11] On this basis, miRNAs may serve as biomarkers for potential applications in cancer diagnosis, prognosis, and prediction. Therefore, effective methods for miRNA detection aroused people's attention in spite of difficulties including similar nucleotide sequences, short length, and low expression associated with miRNAs.

Over the past decade, various analytical methods have been employed to study oligonucleotides detection. The most commonly used methods include colorimetric method,[12,13] fluorescence methods,[14,15] quartz crystal microbalance-based methods,[16] and electrochemical methods.[17] For example, oligonucleotide silver nanoparticle conjugates were carried out for detection of target oligonucleotide with colorimetric analysis for the first time and showed higher sensitivity than oligonucleotide-gold nanoparticle conjugates.[18] Colorimetric method was first introduced by Mirkin[19] and has adapted to detecting various biomolecules. However, the infinitesimal differences in color cannot be distinguished by the naked eye in colorimetry; probes with fluorescence suffer from blinking and photo bleaching; quartz crystal microbalance is complicated to operate and hard to generalize; and the signals obtained from bulk nanoparticles concealed individual differences of each nanoparticle. Differences between individual nanoparticles, which cannot be avoided in production, lead to different physical and chemical properties, so measurements at the single nanoparticle level revealing the unique function of individual particles are becoming the trend.

Plasmonics is a promising research branch that has attracted much attention due to its omnifarious applications in molecular

Received: October 18, 2014
Accepted: December 29, 2014
Published: December 29, 2014

DOI: 10.1021/am507218g
ACS Appl. Mater. Interfaces 2015, 7, 2459−2466

rulers,[20] heavy metal ions detection,[21−23] gas molecular detection,[24] membrane transfer applications,[25] and photothermic therapy.[26] These applications are based on the surface plasmon resonance (SPR) of noble metal nanoparticles, which have large negative real and small positive imaginary dielectric constants. Moreover, signals obtained from a single nanoparticle can provide even more detailed information. Therefore, research at single nanoparticle level aroused much attention. For example, the growth process of single Ag@Hg nanoalloy was real-time monitored and presented a color change of scattering spectra from red to white-yellow.[27] Single plasmon nanoparticle sensor developed rapidly on the basis of surface plasmon resonance scattering (SPRS) analytical technique of dark-field light scattering spectroscopy using dark-field microscopy, which has been considered the most straightforward mean to probe chemical reactions,[28] real-time optical sensing with high sensitivity, and the in vivo imaging of cancer cells.[29−31] This technique has been used to study gas sensing[24,32] and nanoparticle growth process[27] due to its high spectral resolution, lower absolute detection limit, and high signal-to-noise ratio. Compared to normal SPR sensors using thin films, single plasmonic nanoparticle sensors have a promising application in nanoparticle tracking and cell imaging.[33−36] However, single plasmonic nanoparticle for the detection of biomolecules confined to the simple adsorption process. For example, single gold nanorod was used to detect single unlabeled proteins on a millisecond time scale through improved plasmon spectroscopy technique which including intense light source and a tailored nanoparticle geometry.[37]

In this study, we describe a simple and selective biosensor based on individual gold nanoparticle (GNP) modified single strand DNA (ssDNA) with a −SH labeled at its 3′ end for assembly on the surface of GNPs. The probe (42 bases) was longer than the target DNA or miRNA (22 bases). The 5′ end of the probe ssDNA (5′-3′, No. 6−27) was complementary to target oligonucleotides and probe ssDNA can form a hairpin on the metal surface. When the GNP-DNA was incubated with target solution, the hairpin structure broke, and target oligonucleotides were captured, resulting in the change of dielectric constant of GNP surface. With the help of SPRS spectroscopy and dark-field microscopy (DFM), hybridization processes of label-free target DNA and miRNA can be real-time monitored at single-nanoparticle level and a red shift of SPRS spectra can be observed. Figure 1 shows the strategy of the

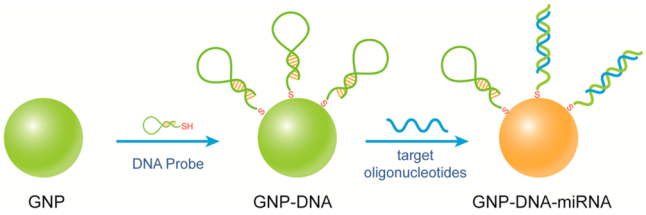

Figure 1. Scheme of GNP-DNA biosensor based on the dielectric constant change caused by hybridization on the single GNP's surface.

detection process. Taking advantage of sensitivity of SPRS spectra, this single nanoparticle biosensor showed excellent selectivity with limit of detection (LOD) up to 3 nM.

EXPERIMENTAL SECTION

Materials and Apparatus. Sodium citrate was purchased from Sigma Company (China). Hydroxylamine-hydrochloride (NH_2OH·HCl) and $HAuCl_4$·$3H_2O$ were purchased from Aladdin Company (China). All chemicals were used without additional purification. All solutions were prepared using ultrapure water obtained from a Milli-Q water purification system (Millipore Corp., Bedford, MA) with resistivity of 18.2 MΩ cm.

All the DNA and RNA sequences used in this study were synthesized and HPLC-purified by Takara Biotechnology Co. (Dalian, China) and used without further purification. The sequences of these oligonucleotides are shown as follows: probe ssDNA, 5′-TGA *CTT CAA CAT CAG TCT GAT AAG CTA* AGT CAT TTT TTT TTT-$(CH_2)_6$-SH-3′; target DNA (complementary DNA), 5′-TAG CTT ATC AGA CTG ATG TTG A-3′; single-base mismatch DNA, 5′-TAG CTT ATC AGA C<u>A</u>G ATG TTG A-3′; random DNA, 5′-GCT ATG TAA CTA TGC TAG GCA C-3′; miRNA-21 (complementary miRNA), 5′-UAG CUU AUC AGA CUG AUG UUG A-3′; single-base mismatch miRNA, 5′-UAG CUU AUC AGA C<u>C</u>G AUG UUG A-3′; random miRNA, 5′-GCU AUG UAA CUA UGC UAG GCA C-3′. The italic fragments of probe ssDNA are complementary sequences to target DNA and miRNA-21. The underlined bases are the mismatched bases. Synthetic DNA and miRNA sequences were dissolved in ultrapure water with autoclaved sterilization and kept frozen.

UV−vis absorption spectra were obtained by a Shimadzu UV3600 spectrophotometer. Scanning electron microscope (SEM) images were collected with S-4800 instrument (Japan). Transmission electron microscope (TEM) images were taken on a JEM 2010 instrument (Japan). All the measurements were performed at room temperature.

Preparation of Gold Nanoparticles. For our experiments, GNPs were synthesized by using seed-growth method following the previously reported method.[38] The size of the GNPs is controlled by changing the reaction condition in the process of seed-growth method. Seed GNPs with average diameter of 20 nm were prepared by using citrate as a reducing agent. Sodium citrate (5 mL, 40 mM) was quickly added into boiling $HAuCl_4$ solution (50 mL, 0.01%) with a color change from modena to dark red in several minutes. The solution was kept boiling for 10 min and then removed from the heater, followed by another 15 min of stirring.

The solution was used as seed solution for the synthesis of GNPs larger than 20 nm. In brief, 1 mL of preformed seed solution was added to 20 mL of water, followed by 0.5 mL of 0.2 M hydroxylamine-hydrochloride (NH_2OH·HCl), which was used as a reducing agent. The mixture was stirred vigorously at room temperature. Then, 3.5 mL of $HAuCl_4$ solution (0.1%) was added to the mixture dropwise until the color of solution turned from red to fuchsia.

Preparation of Sensing Substrate. Indium tin oxide (ITO) glass slides were used as substrate for fabrication of nanobiosensor. Due to the excellent electroconductibility, GNPs immobilized on the ITO substrate can be observed directly without spraying gold film by in situ SEM. For preparation, ITO glass slides were cleaned in an ultrasonic bath by using detergent, acetone, ethanol, and water, sequentially, for 1 h, respectively. Then, the slides were sufficiently rinsed with water and dried with a stream of nitrogen. The cleaned slides were placed in the solution of GNPs, which was diluted 10 times and soaked for 1 min, washed with water and dried with nitrogen. GNPs were modified on the surface of ITO glass slides by physical adsorption.

Immobilization of Single-Strand DNA Probes on GNP Surface of Sensing Substrate. DNA probes were designed to form a hairpin with a thiol group at 3′ ends. Hairpin ssDNA solution (100 μL, 1 μM) was pipetted onto the surface of the ITO glass slide which was modified with GNPs and incubated in the shaker at room temperature overnight at 30 rpm. Then, the ITO glass slide was rinsed with water and dried with nitrogen.

Hybridization Reaction on the Sensor and SPRS Instrumental Asset. Single GNP SPRS spectra were investigated by the dark-field measurements carried out on an inverted microscope (eclipse Ti−U, Nikon, Japan) equipped with a dark-field condenser (0.8 < NA < 0.95), a 20× objective lens, a 100 W halogen lamp to excite the GNPs and generate plasmon resonance scattering light, a true-color digital camera (Nikon DS-fi2) to capture the true color scattering images of GNPs, and a monochromator (Acton SP2300i) equipped

DOI: 10.1021/am507218g
ACS Appl. Mater. Interfaces 2015, 7, 2459−2466

with a spectrograph CCD (PIXIS 400BR: excelon, Princeton Instruments) to obtain the scattering spectra and a grating (grating density, 300 L/mm; blazed wavelength, 500 nm). The true color images of GNPs were taken using a 20× objective lens. The functionalized slide was placed on the automatic stage and 100 μL of target oligonucleotide solution was pipetted onto the surface of the slide. The scattering spectra of the individual nanoparticle were corrected by subtracting the background spectra, which were taken from the adjacent regions without the GNPs and dividing with the calibrated response curve of the entire optical system. The spectra were integrated as 20 s.

X-ray Photoelectron Spectroscopy (XPS). XPS is a surface analytical method due to its sensitivity of the atomic composition with detection limit of outmost 100 Å of a sample surface.[39] XPS analyses of ssDNA adsorption and hybridization with miRNA on the surface of GNPs were performed on an X-ray photoelectronic spectrometer (PHI 5000 VersaProbe, ULVAC-PHI Co., Japan) with an Al Kα X-ray at 1486.6 eV as a light source. High-resolution spectra were acquired, and peak positions were referenced to the C 1s peak at 284.8 eV.

RESULTS AND DISCUSSION

All gold hydrosols were characterized using a UV−vis spectrometer in the wavelength range of 400−700 nm, with a resolution of 0.1 nm. After the addition of chloroauric acid, the GNP absorption peak shifted from 520 to 542 nm (Figure 2B), indicating the growth of GNPs. According to the Mie theory, both the size and the concentration of GNPs can be determined directly from UV−vis spectra, which suggests that the average diameter of GNPs used in the experiments was ~75 nm.[40] This was further proved by TEM images (Figure 2A) and statistical analysis carried out by counting two representative regions of images by using ImageJ software (National Institutes of Health).

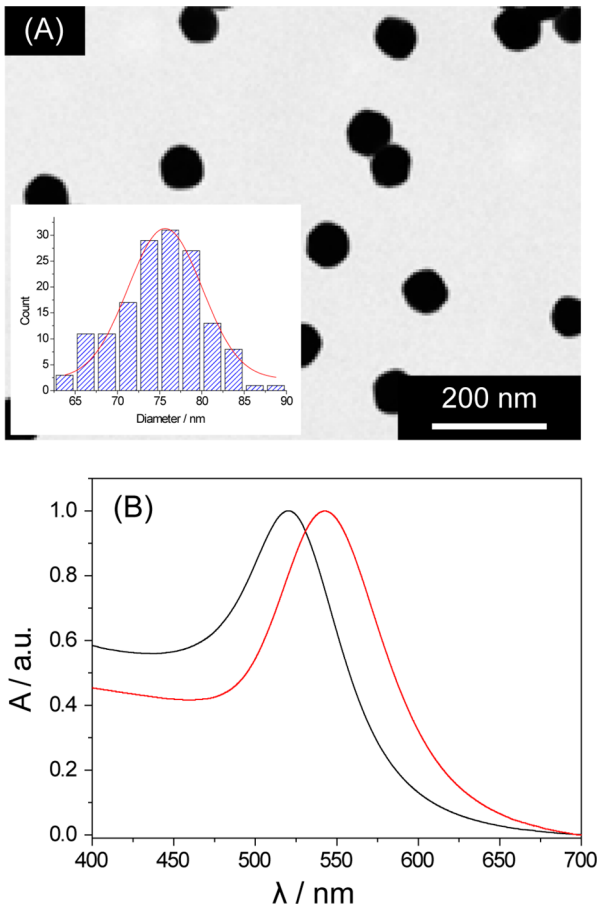

Figure 2. (A) TEM image of GNPs with average diameter of ~75 nm; (B) normalized UV−vis absorption spectra for (black curve) seed solution and (red curve) ~75 nm GNPs.

To compare the morphology of GNPs before and after hybridization, we compared DFM images and in situ SEM images in the experiment. Single GNP immobilized on the ITO glass slide with a mark carved on it was observed through DFM, and color photographs were obtained by color CCD. According to the distance between the single GNP and the mark that was measured by Adobe Photoshop, the ITO glass slide was then observed through SEM and every GNP could be found in the corresponding area of DFM color photographs. Figure 3A shows the DFM image of a typical GNP-DNA immobilized on ITO glass. The in situ SEM images of the selected area in Figure 3A were obtained, which demonstrated that the typical GNP with detailed view was 75 nm in average diameter correspondingly presenting yellow light spot in DFM image. SEM images (Figure 3B,C) of GNP based biosensor were given to compare its shape and size before and after hybridization with target oligonucleotides, demonstrating that there was no change in the shape of GNP during the hybridization process. On the basis of this result, gold sphere nanoparticle with diameter of ~75 nm was chosen to fabricate single nanoparticle biosensor due to its stability of chemical and physical properties.

The adsorption of ssDNA and hybridization between ssDNA and miRNA were assayed by XPS. Table 1 summarizes the XPS atomic percentages of GNP-DNA and GNP-DNA-miRNA. Because pure GNPs did not produce nitrogen or phosphorus signals, the presence of a N 1s peak and a P 2p peak (Figures S3 and S5, Supporting Information) indicate that ssDNA adsorbed onto the gold surface, which also existed in the GNP-DNA-miRNA sample. The sample of GNP-DNA contained 67.71% C, 9.7% N, 17.44% O, 3.42% P, 0.97% S, and 0.77% Au (Table 1). After hybridization with miRNA-21, the content of carbon decreased, as did the phosphorus and sulfur content, while the content of nitrogen and oxygen increased with a composition of 62.64% C, 9.88% N, 23.96% O, 2.07% P, 0.70% S, and 0.72% Au. The experimental atomic ratios (C/N, O/N, P/N) calculated from the element composition changed from 6.98, 1.80, and 0.35 to 6.34, 2.42, and 0.21, respectively. The change tendency of element composition agreed with the theoretical value calculated from pure ssDNA and miRNA-21. Because GNPs were synthesized through seed-growth method, residual sodium citrate resulted in high percentage of C and O.

The XPS spectra of the Au 4f regions for GNP-DNA and GNP-DNA-miRNA samples are shown in Figure S1 (Supporting Information), which presents a $4f_{7/2}$ peak at 84.0 eV and a $4f_{5/2}$ peak at 87.7 eV. The differences between Au $4f_{7/2}$ and Au $4f_{5/2}$ peaks were 3.7 eV, which agrees with the value of zerovalent gold.[41,42] This result suggests that gold atoms stayed in zerovalent state after the adsorption of ssDNA and hybridization with miRNA. Four carbon peaks appeared at 284.8, 286.4, 287.8, and 289.1 eV, respectively, representing different carbon species related to ssDNA (Table 2).

Every individual GNP modified with hairpin ssDNA served as a probe for target DNA detection through hybridization reaction, which could cause a change of the dielectric constant of the surface microenvironment resulting in the shift of GNP's SPRS spectra (Figure 4). A similar phenomenon has shown that when double-stranded DNA attached to a single GNP, plasmon resonance wavelength would change according to the

DOI: 10.1021/am507218g
ACS Appl. Mater. Interfaces 2015, 7, 2459−2466

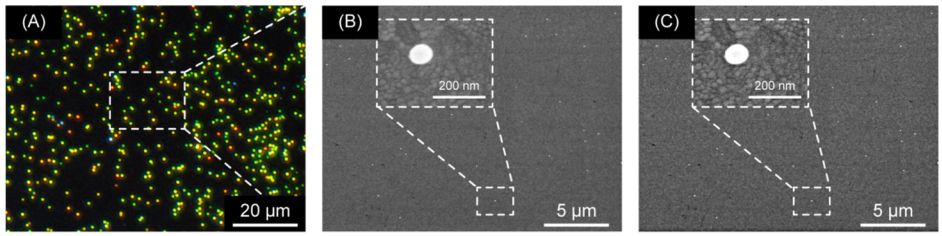

Figure 3. . (A) Representational dark-field image of GNP-DNA before hybridization with miRNA on ITO glass slide. In-situ SEM images of GNP-DNA correspond to the selected area in image A and detail view of the selected GNP-DNA (B) before and (C) after hybridization with miRNA.

Table 1. XPS Compositional Data for GNP-DNA and GNP-DNA-miRNA

	atomic percent				atomic ratio		
	C 1s	N 1s	O 1s	P 2p	C/N	O/N	P/N
GNP-DNA	67.71	9.7	17.44	3.42	6.98	1.80	0.35
GNP-DNA-miRNA	62.64	9.88	23.96	2.07	6.34	2.42	0.21

Table 2. XPS High-Resolution Data of GNPs, GNP-DNA, and GNP-DNA-miRNA

	C				Au	
GNP					84.05	87.71
GNP-DNA	284.80	286.35	287.78	289.10	84.01	87.67
GNP-DNA-miRNA	284.86	286.42	287.80	289.00	84.01	87.69

length of the DNA.[43] It is well-known that size of the nanoparticles is one of the most critical influences for LSPR of noble metal nanoparticles. GNPs of smaller than 40 nm diameter presented dimly scattered green light, which is difficult to visualize in DFM, while larger GNPs can present green or even orange scattering color that are visible to naked eye and to which the eye is more sensitive.[44] Meanwhile, GNPs based biosensors have been confirmed to be more sensitive with larger size.[45]

We characterized the sensitivity of single GNP with an average diameter of 75 nm for different concentrations of the target DNA. Single GNP was functionalized by assembling probe ssDNA at the surface to form GNP-DNA probe. Different times for modifying ssDNA on the surface of GNP were tested for detection of target miRNA-21 with concentration of 1 μM, and the result showed that $\Delta\lambda$ of SPRS spectra of single nanoparticle achieved the maximum value and then decreased with the time after 4 h (Figure 5). SPRS spectra did not show an obvious shift for lack of probe ssDNA in initial

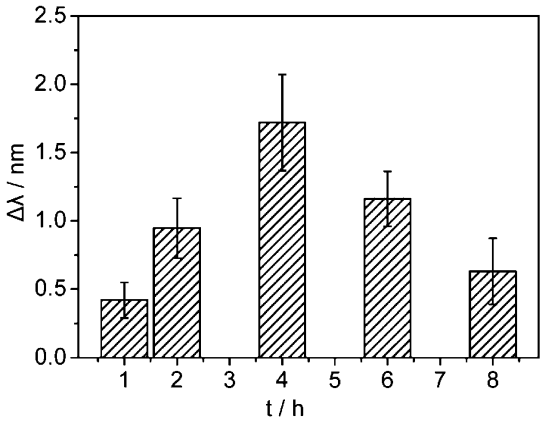

Figure 5. Peak shift of the LSPR scattering spectra of GNP-DNA hybridized with 1 μM of miRNA-21, which were obtained after GNP modified by ssDNA with different time.

stage of ssDNA modification. Long-time modifications induce an overload of probe ssDNA, which prevented the target oligonucleotides from stretching and hybridizing due to steric effect between probe and target molecules. This phenomenon agreed with the results of Steel et al.[46] An explanation was given that this may result from the rigid restrictions on duplex formation. For this reason, 4 h of modification of probe ssDNA was performed in our experiment with concentration of 1 μM.

Once the target DNA solution was pipetted onto the surface of the GNP-DNA biochip, the SPRS spectra of single GNP were obtained continuously in 2 h by DMF equipped with monochromator. Typical SPRS spectra are presented in Figure

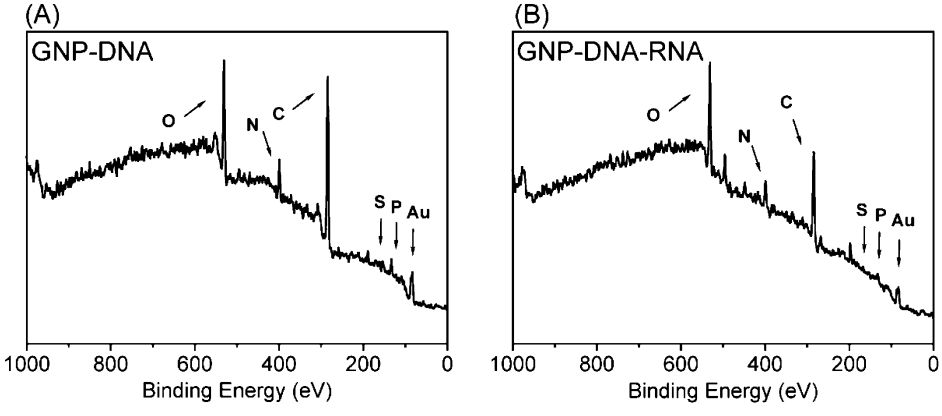

Figure 4. XPS full spectra of (A) GNP-DNA and (B) GNP-DNA-miRNA.

DOI: 10.1021/am507218g
ACS Appl. Mater. Interfaces 2015, 7, 2459−2466

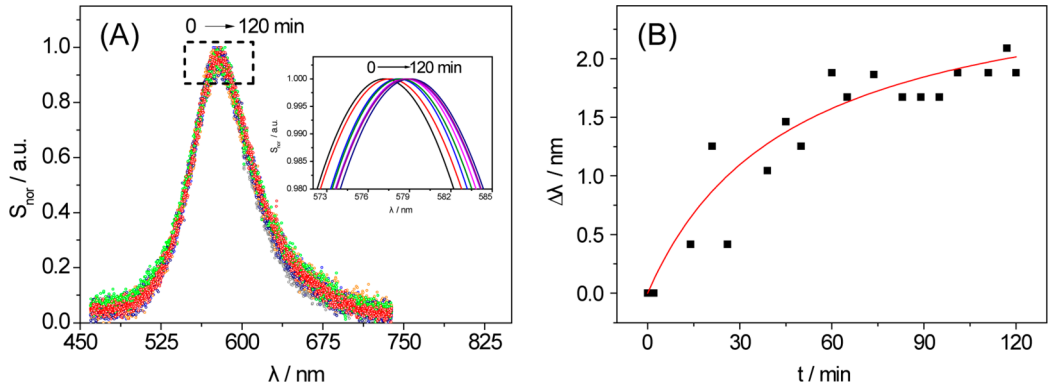

Figure 6. (A) Corresponding LSPR scattering spectra of the selected GNP-DNA incubating with target solution at different time. (B) The plots of LSPR spectra versus time for the selected GNP-DNA with 10 μM of miRNA-21.

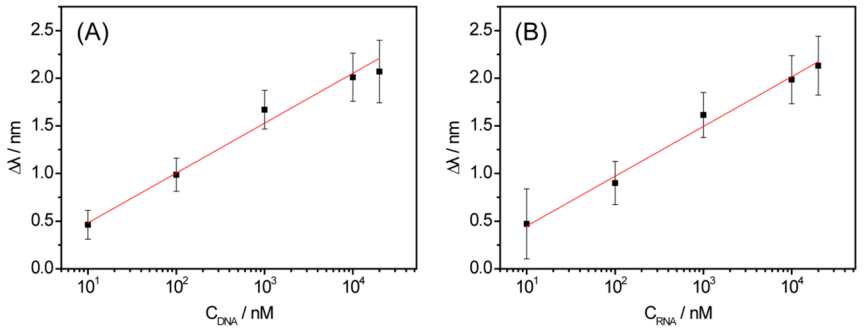

Figure 7. Calibration curve corresponding to the peak shift of the LSPR scattering spectra for target (A) DNA and (B) miRNA-21 of different concentrations (10 nM, 100 nM, 1 μM, 10 μM, and 20 μM).

6A and demonstrate that a continued red shift occurred during real-time monitoring of single ssDNA-labeled GNP incubated in target DNA with concentration of 10 μM. Figure 6B shows the corresponding plots of LSPR spectra peak position red-shift versus time. It shows that $\Delta\lambda$ of SPRS spectra of single nanoparticle increased rapidly in the initial stage and reached a limitation after 1.5 h with a shift of ~2 nm. This process proved that hybridization occurred between probe ssDNA and target DNA on the surface of individual GNP, which caused subtle change of refractive index at the interface and can be reflected through SPRS spectra.

During the experiment, target DNA can hybridize with probe ssDNA completely when reaction time was extended to 4 h, and similar $\Delta\lambda$ of SPRS spectra of single nanoparticle were obtained with different concentration of target DNA. This phenomenon resulted from the diffusion of target DNA molecules in solution. The $\Delta\lambda$ reached a limit faster at high concentration of target DNA than at lower concentration. The first 2 h of incubation were chosen for our study, and a linear relationship was discovered between $\Delta\lambda$ of SPRS spectra of single nanoparticle and concentrations of target DNA. As shown in Figure 7A, the SPRS spectra shifted proportionally to the target DNA concentration in the range of 10 nM to 20 μM. The shift value decreased with lower concentration and reached the limitation at 10 nM with a 0.4 nm red shift within the margin of error. A linear relationship between $\Delta\lambda$ and concentration of DNA was demonstrated. The regression equation could be expressed as $\Delta\lambda = 0.516 \log C_{DNA} - 0.046$ ($R^2 = 0.9902$) and the limit of detection (LOD) was calculated to be 3 nM when the signal-to-noise ratio is 3. For colorimetric detection of DNA, the limit was 8 nM.[47] For chemiluminescence resonance energy transfer (CRET) detection of DNA, the sensitivity corresponded to 10^{-8} M.[48] For the detection of miRNA, silver nanoclusters/DNA probes were used, and the detection limit was μM level;[14] a similar method has been improved to nM level for the detection of microRNA.[49] For the detection of Hg^{2+}, the largest LSPR response was a shift of ~2.5 nm.[50] Compared to these methods mentioned above, the detection method we used had the advantage of lower LOD.

Furthermore, the selectivity of the individual DNA-based nanosensor was studied. We measured the SPRS spectra of single nanoparticle biosensor when incubating with single-mismatch DNA and random DNA to compare with the shift of SPRS spectra when complementary target DNA was used to incubate with GNP-DNA probe. As shown in Figure 8, the shifts of the SPRS spectra of single plasmonic nanosensor were

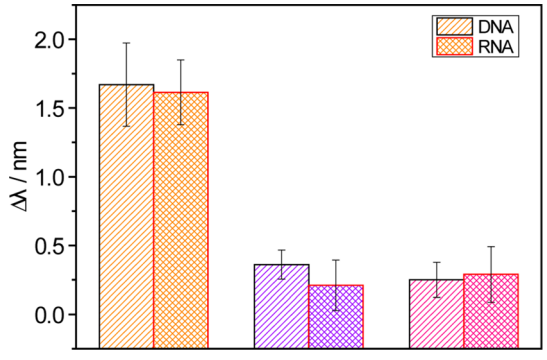

Figure 8. Peak shift of the LSPR scattering spectra of (orange) complementary target, (purple) single-base-mismatched, and (pink) random (diagonal) DNA and (crosshatch) RNA at same concentration of 1 μM.

DOI: 10.1021/am507218g
ACS Appl. Mater. Interfaces 2015, 7, 2459−2466

1.7, 0.4, and 0.2 nm, respectively, in the presence of target, single-mismatch, and random DNA with the same concentration of 1 μM, suggesting that single-mismatch and random DNA can be distinguished by the single plasmonic nanosensor.

On the basis of the above results, single GNP based biosensor can also be used for label-free miRNAs. In our study, miRNA-21was chosen as target miRNA for it has been found in cancers with overexpression[5−10] and regarded as a good candidate as biomarker in cancer. Because Alivisatos et al.[51] has already proved that small difference of buffer solution could affect the peak wavelength of the plasmon resonance of a particle, ultrapure water with autoclaved sterilization was used as solvent for target oligonucleotides to avoid the influence of solvent. The functionalized single nanoparticle sensor presented similar performance for miRNA-21 compared to DNA. As shown in Figure 7B, the SPRS spectra shifted with the addition of miRNA-21. $\Delta\lambda$ can be observed to increase with increasing concentration of target miRNA-21 with a regression equation expressed as $\Delta\lambda$ = 0.53 log C_{RNA} − 0.098 (R^2 = 0.9711). When the concentration of miRNA-21 was 3 nM, the change of SPRS spectra reached a limit. This result predicted a promising application for label-free detection of biomarkers of lung cancer.

To evaluate the selectivity of this single nanoparticle biosensor, we chose three kinds of RNA sequences to incubate with the GNP-DNA probe and hybridize with the probe ssDNA: complementary target miRNA-21, single-mismatch RNA, and random RNA. SPRS spectra were measured during the process. As shown in Figure 8, miRNA-21 can be easily distinguished due to an obvious shift of 1.6 nm of SPRS spectra of single plasmonic nanosensor, compared to respectively 0.2 and 0.3 nm shift of SPRS spectra after incubation with single-mismatch and random RNA with the same concentration of 1 μM. These results implied that the ssDNA functionalized single GNP biosensor was able to discriminate with high specify.

For further exploration of practical application, we assessed the ability of the GNP-DNA based single nanoparticle sensor in fetal bovine serum (FBS). FBS without miRNA-21 was diluted 50 times and used as a blank, which showed almost no shift of the SPRS spectra (Figure S7, Supporting Information). Then analyses of different concentrations of miRNA-21 were performed with 2% FBS (Figure 9). With the addition of miRNA-21, the SPRS spectra presented red shifts as concentrations increased. Compared to miRNA-21 in aqueous solution, calibration curve was similar to the presence of 2% FBS with a regression equation expressed as $\Delta\lambda$ = 0.45 log C_{RNA} + 0.23 (R^2 = 0.9741). The single nanoparticle biosensor can detect miRNA-21 as low as 3 nM in 2% FBS when the signal-to-noise ratio is 3.

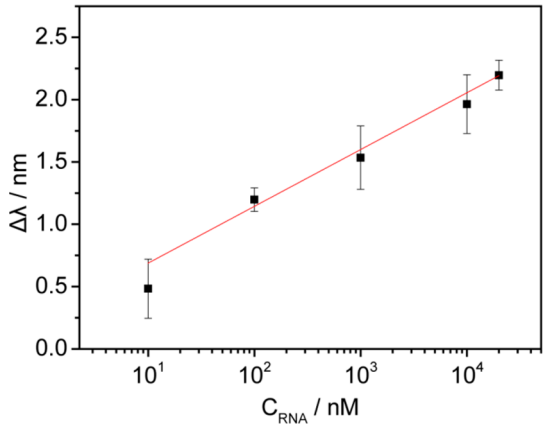

Figure 9. Calibration curve corresponding to the peak shift of the LSPR scattering spectra for miRNA-21 of different concentrations (10 nM, 100 nM, 1 μM, 10 μM, 20 μM) in the serum.

CONCLUSION

In summary, we developed a novel method based on SPR sensor for label-free detection of DNA and miRNA-21 at single nanoparticle level. The GNPs were immobilized onto the ITO glass substrate to form the main part of the sensors. Probe ssDNA was modified on the surface of GNPs through Au−S bond to capture the target oligonucleotides. The signals of SPRS spectra of individual GNP were obtained by using the SPRS instrumental asset, and a red shift was observed during the process of hybridization due to the change of refractive index of the surface of individual GNP. This SPR sensor achieved the detection of 3 nM at single nanoparticle level and showed excellent selectivity for miRNA sequences. Based on these advantages, further development of single nanoparticle based SPR sensors for the detection of multiple oligonucleotides biomarkers has a promising future in the fields of unlabeled biomolecules detection and miRNA diagnostics.

ASSOCIATED CONTENT

Supporting Information

XPS spectra of Au 4f, C 1s, N 1s, O 1s, P 2p, and S 2p for pure GNPs, GNP-DNA, and GNP-DNA-miRNA; plots of LSPR spectra versus time for the selected GNP-DNA with 2% FBS. This material is available free of charge via the Internet at http://pubs.acs.org.

AUTHOR INFORMATION

Corresponding Authors

*E-mail: iamlzhang@njupt.edu.cn.
*E-mail: iamwhuang@njupt.edu.cn.
*E-mail: iamlhwang@njupt.edu.cn.

Author Contributions

[§]Y.L.H. and L.Z. contributed equally to this work.

Notes

The authors declare no competing financial interest.

ACKNOWLEDGMENTS

For the financial support for this work, we thank the State Plan for Development of Basic Research in Key Areas (No. 2012CB933301), the Ministry of Education of China (IRT1148, NCET-10-0179), the National Natural Science Foundation of China (No. 61205195), the Specialized Research Fund for Doctoral College (Nos. 20093223110003, 20123223120011, 20123223110007), the University Science Research Project of Jiangsu Province (12KJB150018), A Project Funded by the Priority Academic Program Development of Jiangsu Higher Education Institutions, and the Natural Science Foundation of Jiangsu Province, China (BM2012010).

REFERENCES

(1) Ambros, V. The Functions of Animal MicroRNAs. *Nature* **2004**, *431* (7006), 350−355.
(2) Sun, K.; Lai, E. C. Adult-Specific Functions of Animal MicroRNAs. *Nat. Rev. Genet.* **2013**, *14* (8), 535−548.

DOI: 10.1021/am507218g
ACS Appl. Mater. Interfaces 2015, 7, 2459−2466

(3) Giraldez, A. J.; Cinalli, R. M.; Glasner, M. E.; Enright, A. J.; Thomson, J. M.; Baskerville, S.; Hammond, S. M.; Bartel, D. P.; Schier, A. F. MicroRNAs Regulate Brain Morphogenesis in Zebrafish. *Science* **2005**, *308* (5723), 833−838.
(4) Iorio, M. V.; Ferracin, M.; Liu, C. G.; Veronese, A.; Spizzo, R.; Sabbioni, S.; Magri, E.; Pedriali, M.; Fabbri, M.; Campiglio, M.; Menard, S.; Palazzo, J. P.; Rosenberg, A.; Musiani, P.; Volinia, S.; Nenci, I.; Calin, G. A.; Querzoli, P.; Negrini, M.; Croce, C. M. MicroRNA Gene Expression Deregulation in Human Breast Cancer. *Cancer Res.* **2005**, *65* (16), 7065−7070.
(5) Takamizawa, J.; Konishi, H.; Yanagisawa, K.; Tomida, S.; Osada, H.; Endoh, H.; Harano, T.; Yatabe, Y.; Nagino, M.; Nimura, Y.; Mitsudomi, T.; Takahashi, T. Reduced Expression of the Let-7 MicroRNAs in Human Lung Cancers in Association with Shortened Postoperative Survival. *Cancer Res.* **2004**, *64* (11), 3753−3756.
(6) Dillhoff, M.; Liu, J.; Frankel, W.; Croce, C.; Bloomston, M. MicroRNA-21 is Overexpressed in Pancreatic Cancer and a Potential Predictor of Survival. *J. Gastrointest. Surg.* **2008**, *12* (12), 2171−2176.
(7) Meng, F. Y.; Henson, R.; Wehbe-Janek, H.; Ghoshal, K.; Jacob, S. T.; Patel, T. MicroRNA-21 Regulates Expression of the PTEN Tumor Suppressor Gene in Human Hepatocellular Cancer. *Gastroenterology* **2007**, *133* (2), 647−658.
(8) Asangani, I. A.; Rasheed, S. A. K.; Nikolova, D. A.; Leupold, J. H.; Colburn, N. H.; Post, S.; Allgayer, H. MicroRNA-21 (miR-21) Post-Transcriptionally Downregulates Tumor Suppressor Pdcd4 and Stimulates Invasion, Intravasation, and Metastasis in Colorectal Cancer. *Oncogene* **2008**, *27* (15), 2128−2136.
(9) Chan, J. A.; Krichevsky, A. M.; Kosik, K. S. MicroRNA-21 is an Antiapoptotic Factor in Human Glioblastoma Cells. *Cancer Res.* **2005**, *65* (14), 6029−6033.
(10) Bottoni, A.; Piccin, D.; Tagliati, F.; Luchin, A.; Zatelli, M. C.; Uberti, E. C. D. MiR-15a and MiR-16−1 Down-Regulation in Pituitary Adenomas. *J. Cell. Physiol.* **2005**, *204* (1), 280−285.
(11) Gao, W.; Shen, H.; Liu, L. X.; Xu, J. A.; Xu, J.; Shu, Y. Q. MiR-21 Overexpression in Human Primary Squamous Cell Lung Carcinoma is Associated with Poor Patient Prognosis. *J. Cancer Res. Clin. Oncol.* **2011**, *137* (4), 557−566.
(12) Zhou, Z.; Wei, W.; Zhang, Y.; Liu, S. DNA-Responsive Disassembly of AuNP Aggregates: Influence of Nonbase-Paired Regions and Colorimetric DNA Detection by Exonuclease III Aided Amplification. *J. Mater. Chem. B* **2013**, *1* (22), 2851−2858.
(13) Zhao, Y. X.; Chen, F.; Lin, M. L.; Fan, C. H. A Methylation-Blocked Cascade Amplification Strategy for Label-Free Colorimetric Detection of DNA Methyltransferase Activity. *Biosens. Bioelectron.* **2014**, *54*, 565−570.
(14) Shah, P.; Rorvig-Lund, A.; Ben Chaabane, S.; Thulstrup, P. W.; Kjaergaard, H. G.; Fron, E.; Hofkens, J.; Yang, S. W.; Vosch, T. Design Aspects of Bright Red Emissive Silver Nanoclusters/DNA Probes for MicroRNA Detection. *ACS Nano* **2012**, *6* (10), 8803−8814.
(15) Yang, S. W.; Vosch, T. Rapid Detection of MicroRNA by a Silver Nanocluster DNA Probe. *Anal. Chem.* **2011**, *83* (18), 6935−6939.
(16) Pavlov, V.; Willner, I.; Dishon, A.; Kotler, M. Amplified Detection of Telomerase Activity Using Electrochemical and Quartz Crystal Microbalance Measurements. *Biosens. Bioelectron.* **2004**, *20* (5), 1011−1021.
(17) Kilic, T.; Topkaya, S. N.; Ariksoysal, D. O.; Ozsoz, M.; Ballar, P.; Erac, Y.; Gozen, O. Electrochemical Based Detection of MicroRNA, Mir21 in Breast Cancer Cells. *Biosens. Bioelectron.* **2012**, *38* (1), 195−201.
(18) Thompson, D. G.; Enright, A.; Faulds, K.; Smith, W. E.; Graham, D. Ultrasensitive DNA Detection Using Oligonucleotide−Silver Nanoparticle Conjugates. *Anal. Chem.* **2008**, *80* (8), 2805−2810.
(19) Elghanian, R.; Storhoff, J. J.; Mucic, R. C.; Letsinger, R. L.; Mirkin, C. A. Selective Colorimetric Detection of Polynucleotides Based on the Distance-Dependent Optical Properties of Gold Nanoparticles. *Science* **1997**, *277* (5329), 1078−1081.
(20) Yang, L. L.; Wang, H. Y.; Yan, B.; Reinhard, B. M. Calibration of Silver Plasmon Rulers in the 1−25 nm Separation Range: Experimental Indications of Distinct Plasmon Coupling Regimes. *J. Phys. Chem. C* **2010**, *114* (11), 4901−4908.
(21) Wang, L.; Li, T.; Du, Y.; Chen, C. G.; Li, L.; Zhou, M.; Dong, S. J. Au NPs-enhanced Surface Plasmon Resonance for Sensitive Detection of Mercury(II) Ions. *Biosens. Bioelectron.* **2010**, *25* (12), 2622−2626.
(22) Zhang, H. Y.; Yang, L. Q.; Zhou, B. J.; Liu, W. M.; Ge, J. E. C.; Wu, J. S.; Wang, Y.; Wang, P. F. Ultrasensitive and Selective Gold Film-based Detection of Mercury (II) in Tap Water Using a Laser Scanning Confocal Imaging-Surface Plasmon Resonance System in Real Time. *Biosens. Bioelectron.* **2013**, *47*, 391−395.
(23) Lin, T. J.; Chung, M. F. Detection of Cadmium by a Fiber-Optic Biosensor Based on Localized Surface Plasmon Resonance. *Biosens. Bioelectron.* **2009**, *24* (5), 1213−1218.
(24) Xiong, B.; Zhou, R.; Hao, J. R.; Jia, Y. H.; He, Y.; Yeung, E. S. Highly Sensitive Sulphide Mapping in Live Cells by Kinetic Spectral Analysis of Single Au-Ag Core-Shell Nanoparticles. *Nat. Commun.* **2013**, *4*, 1−9.
(25) Braun, T.; Ghatkesar, M. K.; Backmann, N.; Grange, W.; Boulanger, P.; Letellier, L.; Lang, H. P.; Bietsch, A.; Gerber, C.; Hegner, M. Quantitative Time-Resolved Measurement of Membrane Protein-Ligand Interactions Using Microcantilever Array Sensors. *Nat. Nanotechnol.* **2009**, *4* (3), 179−185.
(26) Mayer, K. M.; Hafner, J. H. Localized Surface Plasmon Resonance Sensors. *Chem. Rev.* **2011**, *111* (6), 3828−3857.
(27) Liu, Y.; Huang, C. Z. Real-Time Dark-Field Scattering Microscopic Monitoring of the in Situ Growth of Single Ag@Hg Nanoalloys. *ACS Nano* **2013**, *7* (12), 11026−11034.
(28) Shi, L.; Jing, C.; Ma, W.; Li, D. W.; Halls, J. E.; Marken, F.; Long, Y. T. Plasmon Resonance Scattering Spectroscopy at the Single-Nanoparticle Level: Real-Time Monitoring of a Click Reaction. *Angew. Chem., Int. Ed.* **2013**, *52* (23), 6011−6014.
(29) El-Sayed, I. H.; Huang, X. H.; El-Sayed, M. A. Surface Plasmon Resonance Scattering and Absorption of Anti-EGFR Antibody Conjugated Gold Nanoparticles in Cancer Diagnostics: Applications in Oral Cancer. *Nano Lett.* **2005**, *5* (5), 829−834.
(30) Austin, L. A.; Kang, B.; Yen, C. W.; El-Sayed, M. A. Plasmonic Imaging of Human Oral Cancer Cell Communities During Programmed Cell Death by Nuclear-Targeting Silver Nanoparticles. *J. Am. Chem. Soc.* **2011**, *133* (44), 17594−17597.
(31) Kang, B.; Austin, L. A.; El-Sayed, M. A. Real-Time Molecular Imaging throughout the Entire Cell Cycle by Targeted Plasmonic-Enhanced Rayleigh/Raman Spectroscopy. *Nano Lett.* **2012**, *12* (10), 5369−5375.
(32) Liu, N.; Tang, M. L.; Hentschel, M.; Giessen, H.; Alivisatos, A. P. Nanoantenna-Enhanced Gas Sensing in a Single Tailored Nanofocus. *Nat. Mater.* **2011**, *10* (8), 631−636.
(33) Zhang, L.; Li, Y.; Li, D. W.; Jing, C.; Chen, X. Y.; Lv, M.; Huang, Q.; Long, Y. T.; Willner, I. Single Gold Nanoparticles as Real-Time Optical Probes for the Detection of NADH-Dependent Intracellular Metabolic Enzymatic Pathways. *Angew. Chem., Int. Ed.* **2011**, *50* (30), 6789−6792.
(34) Rong, G. X.; Wang, H. Y.; Skewis, L. R.; Reinhard, B. M. Resolving Sub-Diffraction Limit Encounters in Nanoparticle Tracking Using Live Cell Plasmon Coupling Microscopy. *Nano Lett.* **2008**, *8* (10), 3386−3393.
(35) Louit, G.; Asahi, T.; Tanaka, G.; Uwada, T.; Masuhara, H. Spectral and 3-Dimensional Tracking of Single Gold Nanoparticles in Living Cells Studied by Rayleigh Light Scattering Microscopy. *J. Phys. Chem. C* **2009**, *113* (27), 11766−11772.
(36) Li, Y.; Jing, C.; Zhang, L.; Long, Y. T. Resonance Scattering Particles as Biological Nanosensors in Vitro and in Vivo. *Chem. Soc. Rev.* **2012**, *41* (2), 632−642.
(37) Ament, I.; Prasad, J.; Henkel, A.; Schmachtel, S.; Sonnichsen, C. Single Unlabeled Protein Detection on Individual Plasmonic Nanoparticles. *Nano Lett.* **2012**, *12* (2), 1092−1095.

DOI: 10.1021/am507218g
ACS Appl. Mater. Interfaces 2015, 7, 2459−2466

(38) Brown, K. R.; Walter, D. G.; Natan, M. J. Seeding of Colloidal Au Nanoparticle Solutions. 2. Improved Control of Particle Size and Shape. *Chem. Mater.* **2000**, *12* (2), 306−313.
(39) Lee, C. Y.; Gong, P.; Harbers, G. M.; Grainger, D. W.; Castner, D. G.; Gamble, L. J. Surface Coverage and Structure of Mixed DNA/Alkylthiol Monolayers on Gold: Characterization by XPS, NEXAFS, and Fluorescence Intensity Measurements. *Anal. Chem.* **2006**, *78* (10), 3316−3325.
(40) Haiss, W.; Thanh, N. T. K.; Aveyard, J.; Fernig, D. G. Determination of Size and Concentration of Gold Nanoparticles from UV−Vis Spectra. *Anal. Chem.* **2007**, *79* (11), 4215−4221.
(41) *Handbook of X-ray Photoelectron Spectroscopy*, Chastain, J., King Jr., R. C., Eds.; Physical Electronics, Eden Prairie, MN, 1992.
(42) Han, S. W.; Kim, Y.; Kim, K. Dodecanethiol-Derivatized Au/Ag Bimetallic Nanoparticles: TEM, UV/VIS, XPS, and FTIR Analysis. *J. Colloid Interface Sci.* **1998**, *208* (1), 272−278.
(43) Liu, G. L.; Yin, Y. D.; Kunchakarra, S.; Mukherjee, B.; Gerion, D.; Jett, S. D.; Bear, D. G.; Gray, J. W.; Alivisatos, A. P.; Lee, L. P.; Chen, F. Q. F. A Nanoplasmonic Molecular Ruler for Measuring Nuclease Activity and DNA Footprinting. *Nat. Nanotechnol.* **2006**, *1* (1), 47−52.
(44) Truong, P. L.; Ma, X.; Sim, S. J. Resonant Rayleigh Light Scattering of Single Au Nanoparticles with Different Sizes and Shapes. *Nanoscale* **2014**, *6* (4), 2307−2315.
(45) Tu, M. H.; Sun, T.; Grattan, K. T. V. Optimization of Gold-Nanoparticle-Based Optical Fibre Surface Plasmon Resonance (SPR)-Based Sensors. *Sens. Actuators B* **2012**, *164* (1), 43−53.
(46) Steel, A. B.; Herne, T. M.; Tarlov, M. J. Electrochemical Quantitation of DNA Immobilized on Gold. *Anal. Chem.* **1998**, *70* (22), 4670−4677.
(47) Thavanathan, J.; Huang, N. M.; Thong, K. L. Colorimetric Detection of DNA Hybridization Based on a Dual Platform of Gold Nanoparticles and Graphene Oxide. *Biosens. Bioelectron.* **2014**, *55*, 91−98.
(48) Freeman, R.; Liu, X. Q.; Willner, I. Chemiluminescent and Chemiluminescence Resonance Energy Transfer (CRET) Detection of DNA, Metal Ions, and Aptamer-Substrate Complexes Using Hemin/G-Quadruplexes and CdSe/ZnS Quantum Dots. *J. Am. Chem. Soc.* **2011**, *133* (30), 11597−11604.
(49) Xia, X. D.; Hao, Y. Q.; Hu, S. Q.; Wang, J. X. Hairpin DNA Probe with 5′-TCC/CCC-3′ Overhangs for the Creation of Silver Nanoclusters and MiRNA Assay. *Biosens. Bioelectron.* **2014**, *51*, 36−39.
(50) Song, H. D.; Choi, I.; Yang, Y. I.; Hong, S.; Lee, S.; Kang, T.; Yi, J. Picomolar Selective Detection of Mercuric Ion (Hg^{2+}) Using a Functionalized Single Plasmonic Gold Nanoparticle. *Nanotechnology* **2010**, *21* (14), 1−6.
(51) Sonnichsen, C.; Reinhard, B. M.; Liphardt, J.; Alivisatos, A. P. A Molecular Ruler Based on Plasmon Coupling of Single Gold and Silver Nanoparticles. *Nat. Biotechnol.* **2005**, *23* (6), 741−745.

DOI: 10.1021/am507218g
ACS Appl. Mater. Interfaces 2015, 7, 2459−2466